

# Finite element method in applications of magnetohydrodynamics

KAREL FRAŇA

Technical University of Liberec  
Department of Power Engineering  
Halkova 6, 461 17 Liberec  
Czech Republic  
karel.frana@seznam.cz

JÖRG STILLER

Dresden University of Technology  
Institute of Aerospace Engineering  
D-01062  
Germany  
joerg.stiller@tu-dresden.de

*Abstract:* The magnetically induced flow was examined numerically using a computational code based on the finite element method with the streamline-upwind/pressure-stabilized Petrov-Galerkin approach. The mathematical model considers an incompressible unsteady flow with a low frequency and low induction magnetic field. The validation of the magnetic force calculation was carried out on a cylindrical cavity, where the time-dependent electric potential and current density distribution can be derived analytically. The flow under the rotating magnetic field was simulated for the axisymmetric cylindrical and non-axisymmetric square cavity. The effect of the different geometries on the distribution of the time-averaged magnetic force and magnetically driven rotating flow was discussed.

*Key-Words:* finite element methods, stabilization techniques, magnetic forces, rotating flows

## 1 Introduction

Various kind of magnetic fields such as rotating (RMF) or traveling magnetic field (TMF) are successfully applied in metallurgical and single crystal growth processes. In order to use these techniques effectively, an in-depth knowledge about effects of the magnetic field on electrically conducting fluids is needed to understand. The fact, that experimental approaches are mostly too expensive for such investigations so that a numerical simulation was found to be an attractive way for extensive magnetically driven flow studies. An overview of results achieved mainly by numerical simulations can be found e.g. in [1],[3],[5],[8] and [9].

To carry out a numerical simulation of magnetically controlled flows, a computational code extended about magnetohydrodynamic equations is required for comprehensive flow simulations. In the frame of following sections, the numerical computational code based on the finite element method as well as main results achieved by these numerical simulations will be presented.

## 2 Problem formulations

The container, bound by electrically insulated walls with the radius  $R$  (cylindrical container) or half side length  $A$  and the height  $H$ , is filled by an electrically conducting fluid with the density  $\rho$ , kinematical viscosity  $\nu$  and electrical conductivity  $\sigma$ . The fluid inside

is stirred by the rotating magnetic field with a magnetic induction  $\mathbf{B}$  and frequency  $\omega$ . The incompressible viscous flow is governed by the Navier-Stokes equation and the continuity equation taking a form as

$$\frac{\partial \mathbf{u}}{\partial t} + \nabla \cdot \mathbf{u}\mathbf{u} = -\nabla p + \nabla^2 \mathbf{u} + \mathbf{f} \quad (1)$$

$$\nabla \cdot \mathbf{u} = 0 \quad (2)$$

with Dirichlet and Neumann type boundary conditions

$$\mathbf{u} = \mathbf{g} \quad \text{at} \quad \Gamma_g \quad (3)$$

$$\mathbf{n} \cdot (p + \nu \nabla \mathbf{u}) = \mathbf{h} \quad \text{at} \quad \Gamma_h \quad (4)$$

where the velocity  $\mathbf{u}$  and time  $t$  are scaled by  $\nu/A$ ,  $A^2/\nu$ , the pressure  $p$  by  $\nu^2/A^2$  and an external mean body force  $\mathbf{f}$  is scaled by  $\nu^2/A^3$ .

For the calculation of the magnetic body force, the low-frequency and the low-induction RMF condition are assumed. To satisfy these conditions, the magnetic Reynolds number  $Rm$  and the shielding parameter  $S$  have to be in relation that  $Rm = \mu\sigma uR \ll S = \mu\sigma\omega R \leq 1$ , where  $\mu$  denotes the magnetic permeability. Using Ohm's law, the body force takes this form

$$\mathbf{f} = \mathbf{j} \times \mathbf{B} = [\sigma(-\nabla\Phi - \frac{\partial \mathbf{A}}{\partial t} + \mathbf{u} \times \mathbf{B})] \times \mathbf{B} \quad (5)$$

where  $\Phi$  and  $\mathbf{A}$  denote the electric potential and the vector potential, and  $\mathbf{j}$  is the current density. To determine the electric potential  $\Phi$  in Eqn. 5, we can exploit that  $\nabla \cdot \mathbf{j} = 0$  and at boundaries  $\mathbf{j} \cdot \mathbf{n} = 0$ . Thus, the equation for electric potential derived on the basis of Ohm's law is in this form

$$\nabla^2 \cdot \Phi = -\nabla \cdot \left[ \frac{\partial \mathbf{A}}{\partial t} - (\mathbf{u} \times \mathbf{B}) \right] = 0 \quad (6)$$

with the Neumann type boundary condition

$$\frac{\partial \Phi}{\partial n} = -\frac{\partial A_n}{\partial t} \quad (7)$$

For the infinite-length container,  $\partial \Phi / \partial n = 0$ , otherwise  $\partial \Phi / \partial n = -\partial A_n / \partial t$ .

Practically, the time-dependent Lorentz force distribution is computed using Eqns. 5, 6 and 7. Nevertheless, this body force can be divided further into two parts; the time-dependent and the mean part, respectively. Under considerations that the interaction parameter is  $N = \sigma B^2 / \rho \omega \ll 1$  only the mean part of the magnetic body force has a significant effect on the magnetically induced fluid flow and the fluctuating part can be neglected [2] and [4]. The time-averaged part is defined as follows

$$\mathbf{f}_{avg} = \sum_0^{\pi/\omega} \mathbf{f} dt = \frac{1}{M} \sum_{i=1}^M \mathbf{f}_i \quad (8)$$

where  $M$  denotes the number of regularly distributed samples used for the time averaging within the half period of the magnetic field oscillation.

### 3 Numerical approaches

The finite element discretization space of  $\Omega$  with boundary  $\Gamma$  is consisted of  $\Omega^e$ , where  $e = 1, 2, \dots, n_{el}$  and  $n_{el}$  is the number of elements. For velocity and pressure, we define the finite element trial function space denoted as  $S_u^h$  and  $S_p^h$ , and weighting function  $v_u^h$  and  $v_p^h$ . These function spaces are selected for  $H_1^h(\Omega)$ , where  $H_1^h(\Omega)$  is the finite-dimension function space over  $\Omega$ . Equation 1 and 2 can be formally integrated in time and is written as follows: find  $\mathbf{u}^h \in S_u^h$  and  $p^h \in S_p^h$  such that  $\forall \mathbf{w}^h \in v_u^h$ ,

$$\forall q^h \in v_p^h$$

$$\begin{aligned} & \int_{\Omega} \mathbf{w}^h \left( \frac{\mathbf{u}^{n+1} - \mathbf{u}^n}{\delta t} + \nabla \cdot \overline{\mathbf{u}\mathbf{u}} - \overline{\mathbf{f}} + \nabla \overline{p} \right) d\Omega \\ & + \int_{\Omega} (\nabla \mathbf{w}^h)^T : \nabla \overline{\mathbf{u}} d\Omega \\ & - \int_{\Gamma} \mathbf{w}^h \cdot \partial_n \overline{\mathbf{u}} d\Gamma + \int_{\Omega} q^h \cdot \mathbf{u}^{n+1} d\Omega \\ & + \sum_{e=1}^{n_{el}} \int_{\Omega^e} (\tau_{SUPG} \overline{\mathbf{u}} \cdot \nabla \mathbf{w}^h) \cdot (\overline{\mathbf{r}}) d\Omega \\ & + \sum_{e=1}^{n_{el}} \int_{\Omega^e} (\tau_{PSPG} \nabla q^h) \cdot (\overline{\mathbf{r}}) d\Omega = 0 \quad (9) \end{aligned}$$

where the residual  $\overline{\mathbf{r}}$  is defined as

$$\overline{\mathbf{r}} = \partial_t \overline{\mathbf{u}} + \nabla \cdot \overline{\mathbf{u}\mathbf{u}} - \overline{\mathbf{f}} - \nabla^2 \overline{\mathbf{u}} + \nabla \overline{p}. \quad (10)$$

The overbar denotes the time averaged over the time interval given by  $t_n$  and  $t_{n+1}$ . To the standard Galerkin formulation of Eqn. 1 and 2; the SUPG (streamline-upwind/Petrov-Galerkin) and PSPG (pressure-stabilizing/Petrov-Galerkin) terms are added. An appropriate choice for  $\tau_{SUPG}$  and  $\tau_{PSPG}$  is given by [7] and [6]. Both stabilization terms represent weighted residuals, and therefore maintain the consistency of the formulation.

The magnetic body force can be trivially calculated if the current density field is known. The right side of the equation 5 is applied for the calculation of the current density field and it is integrated as follows: find  $\mathbf{j}^h \in S_j^h$  such that  $\forall \mathbf{w}^h \in v_j^h$ , where  $S_j^h$  represents the finite element trial function space and  $v_j^h$  weighting function

$$\begin{aligned} & \int_{\Omega} \mathbf{w}^h [\mathbf{j} + \sigma \nabla \Phi + \sigma \frac{\partial \mathbf{A}}{\partial t} - \sigma (\mathbf{u} \times \mathbf{B})] d\Omega \\ & + \int_{\Gamma} \mathbf{w}^h \partial_n \mathbf{j} d\Gamma = 0. \quad (11) \end{aligned}$$

The boundary integral is zero because of  $\mathbf{j} \cdot \mathbf{n} = 0$ . The time derivation of the vector potential is known for a particular type of the magnetic field. The electric potential must be calculated based on Eqn. 6, and after integration takes the form: find  $\Phi^h \in S_{\Phi}^h$  such that  $\forall q^h \in v_{\Phi}^h$ , where  $S_{\Phi}^h$  represents the finite element trial function space and  $v_{\Phi}^h$  weighting function

$$\begin{aligned} & \int_{\Omega} \nabla q^h \cdot [\nabla \Phi + \frac{\partial \mathbf{A}}{\partial t} - (\mathbf{u} \times \mathbf{B})] d\Omega + \int_{\Gamma} q^h \\ & \partial_n [-\nabla \Phi - \frac{\partial \mathbf{A}}{\partial t} + (\mathbf{u} \times \mathbf{B})] d\Gamma = 0 \quad (12) \end{aligned}$$

In this equation, the boundary integral vanishes because of the Neumann type boundary for the electric potential (see Eqn. 7).

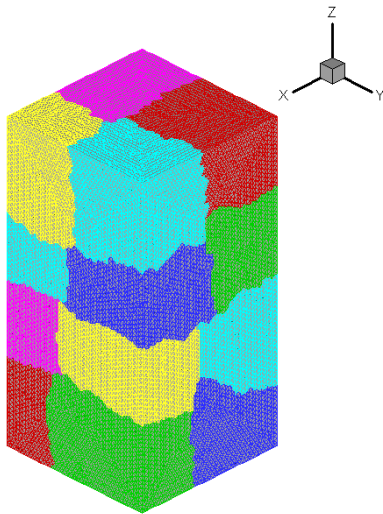


Figure 1: Computational grid decomposed into 16 grid partitions

The integrated Eqn. 9 is further split into a velocity (predictor) and a pressure (corrector) step. The predictor step for velocity is solved explicitly using the Jacobi iterative method, the corrector step involving the pressure equation is solved implicitly by the Conjugated gradient method. The equation 11 and 12 are solved iteratively by the Jacobi method. For the time averages, the second-order Adams-Bashforth method is applied.

The calculation of the mathematical model is fully parallelized. The created computational grid is decomposed into a specific number of partitions using the *METIS* package [11] (see Fig.1). For handling of computational grids, the MG grid library [10] was used which provides a data structure and basic procedures.

### 4 Code validations

The code validation was divided into two significant steps. The first part of the code validation is focused on the mathematical model describing an effect of the magnetic field on the electrically conducting fluids. The second part was dealing with the flow solver itself. The flow solver was validated by various test cases such as unsteady laminar flows in the channel, the Stokes flow in the cylindrical infinite-length containers etc. These tests confirmed the second-order accuracy in space and time. How the code can capture an onset of the flow stability was presented in [3]. Briefly, the results obtained were in good agreement with the results based on high-order computational methods [1].

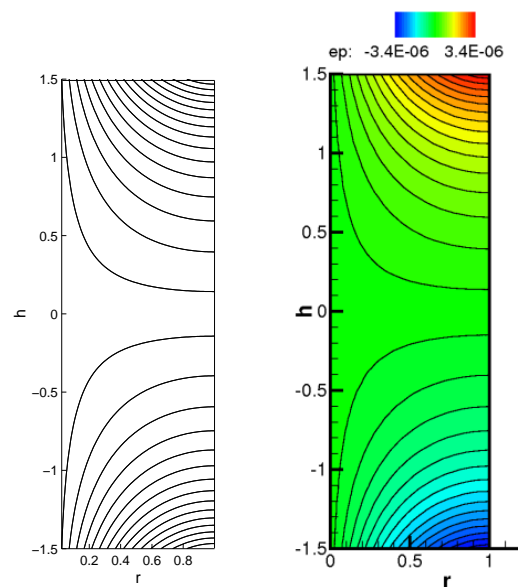


Figure 2: Contours of the electric potential calculated by the analytical form (left) and using the mathematical model (right)

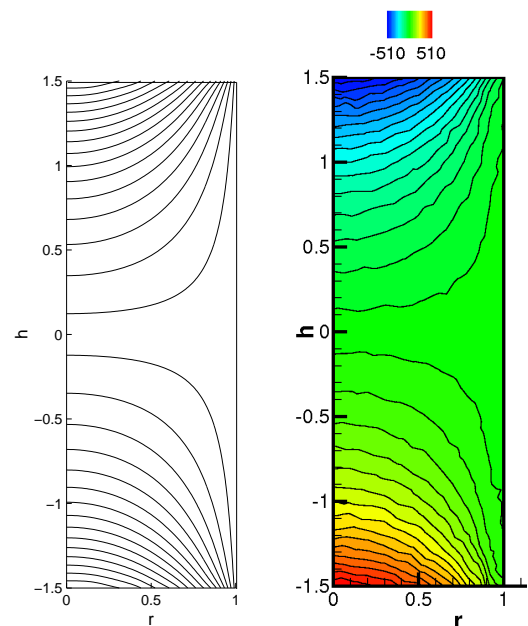


Figure 3: Contours of the y-component of the current density field calculated analytically (left) and using the mathematical model (right) depicted in the yz-slice.

The mathematical model for the magnetic force calculation was examined on the cylindrical finite-length container exposed by a rotating magnetic field. Considering a conducting fluid insight, the current

density and electrical potential can be derived analytically. Figure 2 shows a good agreement of the electric potential distribution calculated, based on the analytical expression and by Equation 12.

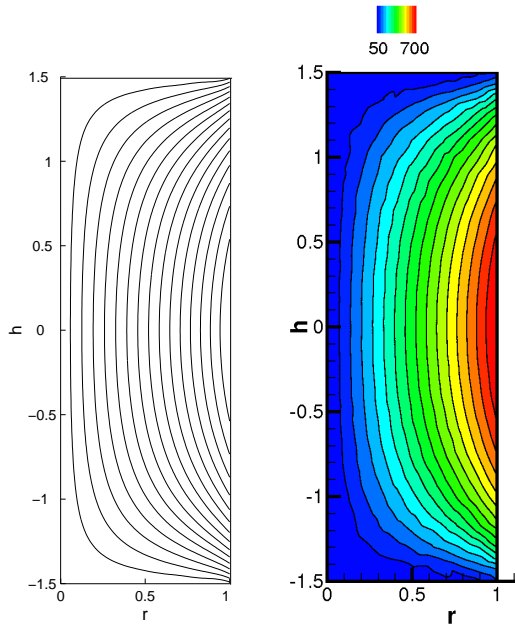


Figure 4: Contours of the z-component of the current density field calculated analytically (left) and using the mathematical model (right) depicted in the yz-slice.

Figure 3 and 4 show a good agreement of the calculated y- and z-components of the time-dependent current density field compared with the analytical solution both in the same time position.

### 5 Results

In order to demonstrate the practical applicability of the computational code for magnetically driven flows, two characteristic examples are chosen: the flow driven by the rotating magnetic field in an axisymmetric and non-axisymmetric cavity respectively. In both cases, the Taylor number  $Ta = 1 \times 10^4$  is considered, where the Taylor number is defined as follows:

$$Ta = \frac{\sigma \omega B_0^2 L^4}{2\rho\nu^2} \tag{13}$$

where  $B_0$  is an amplitude of the magnetic field induction and  $L$  is the characteristic length. The characteristic length is either the radius of the container (cylindrical cavity) or half the side length (square container).

### 5.1 Magnetic force distributions of RMF

The influence of the type of the container on the magnetic force field is demonstrated in Figs. 5 and 6.

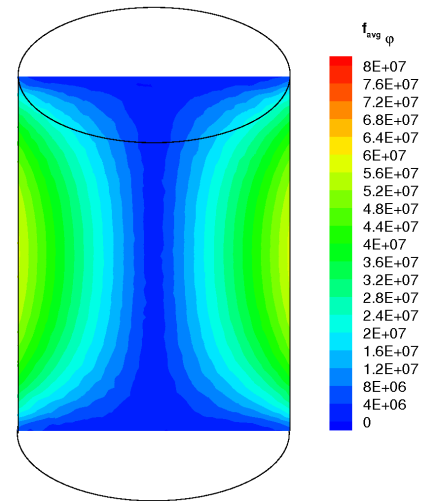


Figure 5: Contours of the Lorentz force in a axisymmetric cavity.

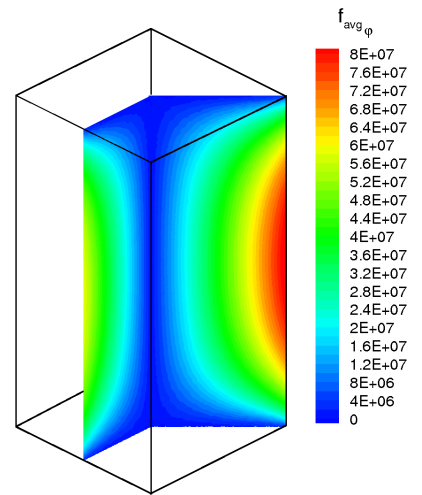


Figure 6: Contours of the Lorentz force in the square container.

In both containers, the maxima of the intensity of the magnetic body force are close to the vertical walls and the contours of the magnetic force distributions look similar. However, as is expected by the magnetic force definition, the intensity of the Lorentz force is higher at the corner of the square container (non-axisymmetric cavity).

### 5.2 The flow driven by the RMF in an axisymmetric cavity

The RMF generates a main rotating flow in the azimuthal direction and due to the imbalance between the magnetic forces and pressure; a weak secondary flow appears in the vertical direction.

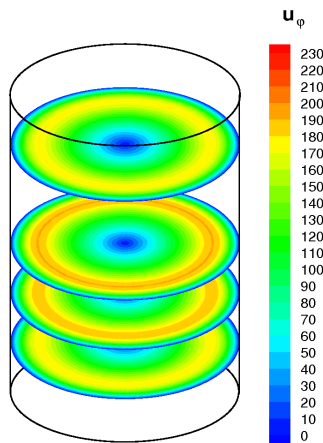


Figure 7: The magnetically driven flows in the cylindrical container.

### 5.3 The flow driven by the RMF in a non-axisymmetric cavity

While the wide range of various flow studies have been carried out in the last decades in the field of the magnetically driven flow in the cylindrical container, other shape of containers stayed behind.

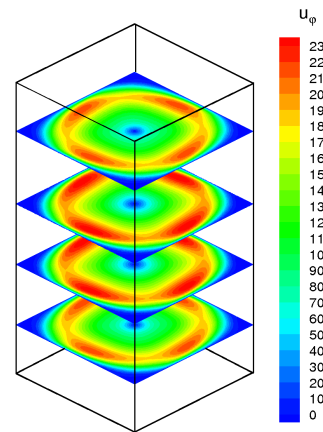


Figure 9: Contours of the rotating flow at horizontal slices in the square container.

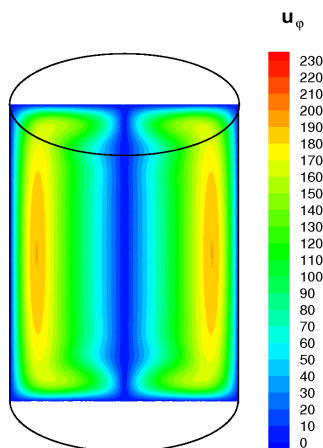


Figure 8: Contours of the rotating flow in the cylindrical cavity.

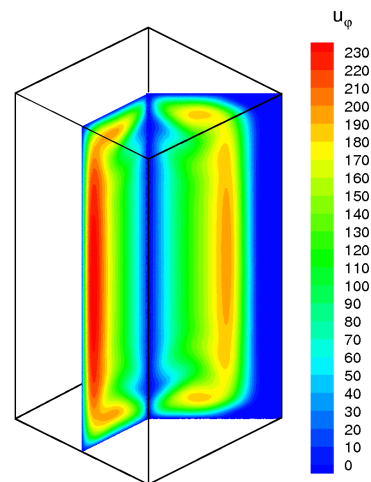


Figure 10: Contours of the rotating flow at the vertical slice in the square container.

Figure 7 and 8 show the main rotating flow in different horizontal slices irregularly extracted along the z-direction and in the vertical slice, respectively. At  $Ta = 1 \times 10^4$ , the velocity field is axisymmetrically and homogeneously distributed. Up to the threshold of the critical Taylor number, the magnetically driven flow remains homogenous and axisymmetric [1]. To find more about magnetically driven flows in the transitional or turbulent flow regime, we refer to our older publications [5] and [3].

One reason of the explanation seems to be a lack of the analytical force formulations. Using the finite-element code presented above, the time-averaged field of the magnetic force can be effectively calculated for any shape of the container. Figures 9 and 10 depict the main rotating flow insight the square container. The contours of the velocity field are similar to the ones found in the cylindrical container, and moreover, weak flow recirculation can be observed in the corner of the container.

## 6 Conclusion

A computational code based on the finite-element method designed especially for the magnetically driven flows was presented. The mathematical model consisted of the Navier-Stokes equations, continuity equation and equations for the calculation of the magnetic field. It was discretized using the Finite-Element Method with SUPG and PSPG stabilization techniques. These numerical approaches were validated on the number of various test cases e.g. cylindrical container, where time-independent magnetic forces, electric current and electric potential can be derived analytically. The practical application of the computational code was presented on the problem of the RMF in two different containers, in the axisymmetric and non-axisymmetric cavity. The significant influence of both the different containers on the magnetic force distribution as well as magnetically driven flows was discussed briefly.

**Acknowledgements:** Financial support from Research Grant MSM 4674788501 Ministry of Education of the Czech Republic and German Deutsche Forschungsgemeinschaft in the frame of the Collaborative Research Center SFB 609 are gratefully acknowledged.

### References:

- [1] I. Grants and G. Gerbeth, Linear three-dimensional instability of a magnetically driven rotating flow, *J. Fluid Mech.* 463, 2002, pp. 229–239.
- [2] L. Martin Witkowski and J.S. Walker, Nonaxisymmetric flow in a finite-length cylinder with a rotating magnetic field, *Physics of Fluids* 11, 1999, pp. 1821–1826.
- [3] J. Stiller, K. Fraňa and A. Cramer, Transitional and weak turbulent flow in a rotating magnetic field, *Physics of Fluids* 19, 2006, 074105
- [4] P.A. Davidson, J.C.R. Hunt, Swirling recirculating flow in a liquid-metal column generated by a rotating magnetic field, *J. Fluid Mech.* 185, 1987, pp. 67–106.
- [5] K. Fraňa, J. Stiller and R. Grundmann, Transitional and turbulent flows driven by a rotating magnetic field, *Magnetohydrodynamics* 42, 2-3, 2006, pp. 187–197.
- [6] T.E. Tezduyar, S. Mittal, S.E. Ray and R. Shih, Incompressible flow computations with stabilized bilinear and linear equal-order-interpolation velocity-pressure elements, *Comput. Meth. Appl. Mech. Eng.* 95, 1992, pp. 211–242.
- [7] T.E. Tezduyar, Y. Osawa, Finite element stabilization parameters computed from element matrices and vectors, *Comput. Meth. Appl. Mech. Eng.* 190, 2001, pp. 411–430.
- [8] P.A. Nikrityuk, K. Eckert and R. Grundmann, Numerical study of a laminar melt flow driven by a rotating magnetic field in enclosed cylinders with different aspect ratios, *Acta Mechanica* 186, 2006, pp. 17–35.
- [9] Yu.M. Gelfgat and J. Priede, MHD flows on a rotating magnetic field (A review), *Magnetohydrodynamics* 31, 1-2, 1995, pp. 188–200
- [10] J. Stiller, W.E. Nagel, MG - A Toolbox for Parallel Grid Adaptation and Implementing Unstructured Multigrid Solvers. In: *E.H. D'Hollander et al. (Eds.): Parallel Computing. Fundamentals and Applications.* Imperial College Press, 2000
- [11] G. Karypis, V. Kumar, Multilevel Algorithms for Multi-Constraint Graph Partitioning, Univ. Minnesota, Dep. Computer Science, TR 98-019, 1998